ACS APPLIED MATERIALS & INTERFACES

Research Article

www.acsami.org

Engineering Schottky Contacts in Open-Air Fabricated Heterojunction Solar Cells to Enable High Performance and Ohmic Charge Transport

Robert L. Z. Hoye,[†] Shane Heffernan,[‡] Yulia Ievskaya,[†] Aditya Sadhanala,[§] Andrew Flewitt,[‡] Richard H. Friend,[§] Judith L. MacManus-Driscoll,[†] and Kevin P. Musselman*[,§,†]

[†]Department of Materials Science and Metallurgy, University of Cambridge, 27 Charles Babbage Road, Cambridge CB3 0FS, United Kingdom

[‡]Electrical Engineering Division, University of Cambridge, 9 JJ Thomson Avenue, Cambridge CB3 0FA, United Kingdom

[§]Department of Physics, University of Cambridge, JJ Thomson Avenue, Cambridge CB3 0HE, United Kingdom

Supporting Information

ABSTRACT: The efficiencies of open-air processed $Cu_2O/Zn_{1-x}Mg_xO$ heterojunction solar cells are doubled by reducing the effect of the Schottky barrier between $Zn_{1-x}Mg_xO$ and the indium tin oxide (ITO) top contact. By depositing $Zn_{1-x}Mg_xO$ with a long band-tail, charge flows through the $Zn_{1-x}Mg_xO$/ITO Schottky barrier without rectification by hopping between the sub-bandgap states. High current densities are obtained by controlling the $Zn_{1-x}Mg_xO$ thickness to ensure that the Schottky barrier is spatially removed from the *p*−*n* junction, allowing the full built-in potential to form, in addition to taking advantage of the increased electrical conductivity of the $Zn_{1-x}Mg_xO$ films with increasing thickness. This work therefore shows that the $Zn_{1-x}Mg_xO$ window layer sub-bandgap state density and thickness are critical parameters that can be engineered to minimize the effect of Schottky barriers on device performance. More generally, these findings show how to improve the performance of other photovoltaic system reliant on transparent top contacts, e.g., CZTS and CIGS.

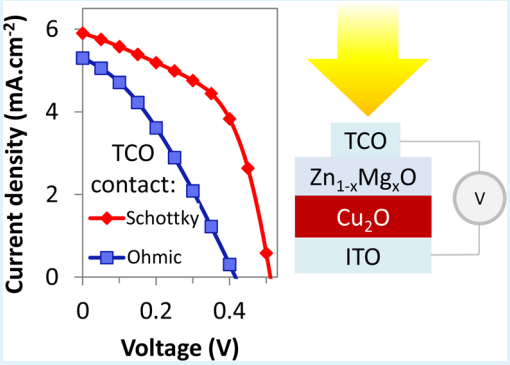

KEYWORDS: *Schottky barrier, Cu_2O solar cells, electrochemical deposition, spatial atmospheric atomic layer deposition, zinc magnesium oxide*

INTRODUCTION

Ideally, heterojunction solar cells should be designed with ohmic contacts at all charge extraction interfaces so that all power losses due to series resistance are minimized, and current densities and fill factors maximized.[1−4] Avoiding Schottky barrier formation is a particularly important consideration in the selection of transparent conducting electrodes (TCE) for the top contacts of solar cells. TCEs admit light to the active layer and conduct charge away, ideally forming an ohmic contact with the semiconductor in order to do so most efficiently.[5] However, other design requirements of TCEs include transparency to visible light, low bulk electrical resistivity and chemical stability.[5,6] Materials properties and fabrication limitations typically restrict the ability to fulfill all design requirements simultaneously. TCEs are commonly oxides (transparent conducting oxides or TCOs), such as indium tin oxide (ITO) and aluminum-doped zinc oxide (AZO).[5] Zinc oxide (ZnO) is a common *n*-type metal oxide employed to form a *p*−*n* junction or act as an electron-selective transport layer in a wide variety of solar cells, including Cu_2O−ZnO, quantum dot, dye-sensitized and hybrid solar cells.[7−11] Although AZO forms an ohmic contact with ZnO (whereas ITO tends to form a Schottky barrier),[5] AZO tends to be less stable than ITO due to the reactive Al dopant,[12] and can be less conductive than ITO.[5] As a result, despite the limitations of the presence of the Schottky barrier,[3] ITO is often deposited on top of ZnO as the transparent top contact layer, such as in CIGS and CZTS solar cells.[13,14] Understanding and finding a means of overcoming the limitations imposed by top contact Schottky barriers is an important challenge that can improve the performance and commercial applicability of the wide variety of solar cells employing these contacts, and is more feasible than finding a new TCO that simultaneously fulfils all design requirements.

In this work, we identify the critical parameters for overcoming the negative effects of Schottky barriers by examining the top contact Schottky interface between zinc magnesium oxide ($Zn_{1-x}Mg_xO$) and ITO in Cu_2O−$Zn_{1-x}Mg_xO$ heterojunction solar cells. Cu_2O solar cells are appealing because they have the potential to reach 20%

Received: August 29, 2014
Accepted: November 24, 2014
Published: November 24, 2014

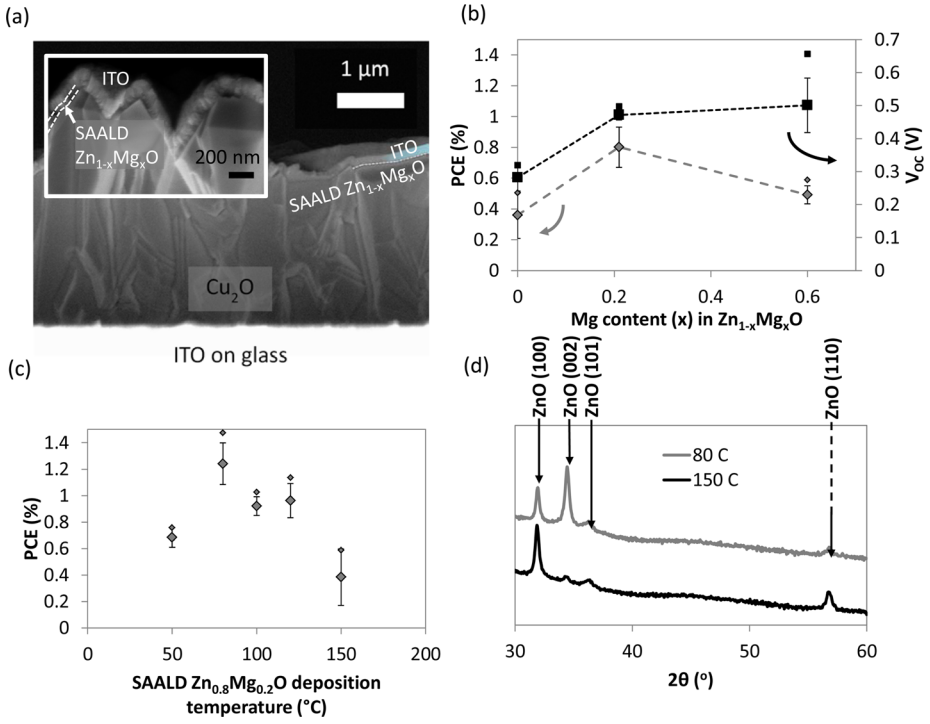

Figure 1. Optimization of 60 nm thick SAALD $Zn_{1-x}Mg_xO$ composition and deposition temperature. (a) Cross-sectional SEM image of a typical glass/ITO/Cu_2O/SAALD $Zn_{1-x}Mg_xO$/sputtered ITO device structure employed in this work. The dashed white line is to indicate the 60 nm thick $Zn_{1-x}Mg_xO$ layer. A close-up on the $Zn_{1-x}Mg_xO$ (layer boundaries indicated by the pair of dashed white lines to guide the eye) is shown inset. (b) Efficiency (PCE) and open-circuit voltage (V_{OC}) of SAALD $Zn_{1-x}Mg_xO$ deposited at 150 °C vs Mg composition (x). (c) PCE vs SAALD $Zn_{0.8}Mg_{0.2}O$ deposition temperature. (d) X-ray diffraction patterns of SAALD $Zn_{0.8}Mg_{0.2}O$ deposited at 80 °C vs 150 °C.

efficiency and Cu_2O itself is a stable, intrinsically *p*-type, nontoxic, earth-abundant material.[15] Because it is challenging to dope Cu_2O to make it *n*-type, much research has been focused on heterojunction architectures, namely Cu_2O/ZnO.[15] ZnO/ITO Schottky barriers are prevalent in these devices,[9,15] making it an ideal system to study Schottky interfaces. $Zn_{1-x}Mg_xO$ instead of ZnO was used in our devices so that we could perform our studies on a system with high performance. Adjusting the amount of Mg incorporated into ZnO allows us to tune the conduction band offset with the Cu_2O absorber and therefore optimize the V_{OC} to maximize the efficiency by reducing V_{OC} losses due to interfacial recombination.[8,16] The ZnO conduction band can also be raised by forming Zn_2TiO_4,[17] but $Zn_{1-x}Mg_xO$ is advantageous because the ZnO conduction band position can be tuned over a wide range.[8] After first optimizing the deposition of $Zn_{1-x}Mg_xO$ onto Cu_2O, we examine how charge can be transported through a Schottky barrier without rectification (like an ohmic contact), before elucidating how the Schottky barrier controls photocurrent densities.

EXPERIMENTAL SECTION

Device Synthesis. The ITO/glass substrates (Colorado Concepts LLC) were roughened by scrubbing with 10 vol % HCl using a cotton bud. These substrates were then cleaned by ultrasonication for 15 min in deionized water, toluene and isopropyl alcohol sequentially. Based on previously reported methods,[18] Cu_2O was deposited galvanostatically at 40 °C under a current density of −1.5 mA·cm^{-2} and a bath pH of 12.65.

SAALD zinc magnesium oxide was deposited based on previously reported methods.[8] For undoped ZnO, the bubbling rate through the diethylzinc precursor was 25 mL·min^{-1}. For $Zn_{0.8}Mg_{0.2}O$, the diethylzinc bubbling rate was 6 mL·min^{-1} and the bis-(ethylcyclopentadienyl)magnesium bubbling rate was 200 mL·min^{-1}. For $Zn_{0.4}Mg_{0.6}O$, the diethylzinc bubbling rate was 5.7 mL·min^{-1} and the bis(ethylcyclopentadienyl)magnesium bubbling rate was 500 mL·min^{-1}. Caution needs to be taken when handling diethylzinc or bis(ethylcyclopentyldienyl)magnesium, because they are pyrophoric and must be stored and handled in an oxygen- and water-free environment, such as a glovebox or gastight container sealed inside a nitrogen-filled glovebox.

Indium tin oxide (ITO) top contacts were deposited by DC magnetron sputtering from a ceramic target (ITO; 10% SnO). The base pressure was 2−8 × 10^{-10} mbar. During sputtering, the power used was 20 W, Ar pressure ∼2.55 Pa. 5 min of sputtering was employed to deposit ∼60 nm ITO (measured using cross-sectional scanning electron microscopy, SEM). A shadow mask was employed so that the overlap between the top and bottom ITO contacts was ∼6 mm^2.

Al-doped ZnO (AZO) was also deposited at room temperature by DC magnetron sputtering from a ceramic target (ZnO; 1 wt % Al). Films were sputtered with flowing argon (35 mL·min^{-1}, operating pressure of 7.4 × 10^{-3} mbar). The maximum base pressure was 3 × 10^{-6} mbar.

Device Characterization. Solar simulations were performed using an Oriel 92250A solar simulator under AM 1.5G illumination, corrected for spectral mismatch. A Keithley 2623A source-measure unit was employed to sweep through the applied biases and measure the current from the cells. Each cell was masked to 4 mm^2 to prevent edge effects. At least five samples were employed for each averaged parameter.

Film Characterization. Cross-sectional scanning electron microscopy (SEM) was performed using a LEO VP-1530 instrument. Impedance spectroscopy was performed using an Agilent 4294 Precision Impedance Analyzer. An oscillating voltage with an amplitude of 0.02 V and a specified series of DC biases was applied from a frequency of 40 Hz to 10 MHz. The impedance magnitude and argument were measured with 201 data points per sweep and recorded using custom-made Labview software. The Nyquist plots were fitted

numerically with the Voigt model to determine the equivalent circuit parameters.

The absorption spectra of the films were obtained using UV−visible spectrophotometry above the bandgap and photothermal deflection spectroscopy (PDS) below the bandgap. The $Zn_{1-x}Mg_xO$ films were deposited onto a quartz substrate. UV−visible spectra were obtained using an Agilent/HP 8453 UV−visible spectrometer. Because interference patterns obscure the sub-bandgap absorption, PDS was employed to measure the film absorption coefficients that were not convoluted with interference patterns.[8] PDS spectra were obtained by immersing the quartz-mounted sample in Fluorinert FC-72. The deflection of a fixed wavelength (670 nm) probe laser beam was measured using a position sensing detector and lock-in detector to measure the absorption at that particular wavelength.

Conductivity measurements on zinc magnesium oxide and Hall measurements on AZO were performed using the van der Pauw method on the metal oxide films deposited on Corning glass using an H-50 and Kepco Bipolar Power Supply Unit from MMR Technologies Inc. The magnetic fields applied during measurements were 0.1 and 0.2 T. The films were deposited on glass square substrates and had indium contacts applied at the four corners after cleaning in isopropyl alcohol and ethanol.

For the ITO films, Hall measurements were also performed using the van der Pauw method, but using a magnetic field of 1 T. The ITO films on borosilicate glass were electrically contacted using silver paste. A Keithley 6220 Precision Current Source was used to apply current to two terminals in the sample and the voltage across the other two terminals measured using a Keithley 2182A Nanovoltmeter.

RESULTS AND DISCUSSION

In this study, the heterojunction was fabricated using two scalable open-air techniques in order to be highly relevant to the ultimate goal of implementing these solar cells on a commercial scale.[19] Electrodeposition was employed for fabricating Cu_2O and spatial atmospheric atomic layer deposition (SAALD)[7] for ZnO. The SAALD ZnO was conformally coated onto 2.5 μm thick Cu_2O electrodeposited on ITO (Figure 1a).

First, we optimized the deposition conditions to achieve high performance and record open-circuit voltages. Although this inverted architecture (as opposed to Cu_2O being deposited on ZnO) has the advantage of greater light absorption due to the highly textured Cu_2O layer,[16] it is limited by the formation of the more thermodynamically stable CuO on the surface of Cu_2O, which can degrade device performances.[19,20] To minimize CuO formation, we (i) lowered the deposition temperature of SAALD $Zn_{1-x}Mg_xO$ from the typical 150 °C[8] to 80 °C (Figure 1c) and (ii) scanned the Cu_2O under flowing vapors of the organometallic precursors from the SAALD gas manifold for five cycles before flowing the oxidant (Figure S1, Supporting Information). These improved the efficiencies from 0.8% to 1.5%. Also, X-ray diffraction measurements show that even when the SAALD $Zn_{1-x}Mg_xO$ deposition temperature was reduced from 150 to 80 °C, the films remained polycrystalline (Figure 1d). We also incorporated Mg into ZnO because the band-alignment of ZnO with Cu_2O is not optimal, which produces a "cliff" in the conduction band offset between the two materials that encourages interfacial recombination and reduces open-circuit voltages (V_{OC}'s).[16,21] By raising the ZnO conduction band through Mg incorporation, the V_{OC} of Cu_2O−$Zn_{1-x}Mg_xO$ devices was increased up to 0.66 V (Figure 1b), which, to our knowledge, is the highest for open-air fabricated heterojunctions based on electrodeposited Cu_2O.[22−24] That the V_{OC} increase was due to a reduction in recombination can be seen from the reduction in the reverse bias saturation current densities (Figure S2a, Supporting Information) with increasing Mg contents. The highest efficiencies were obtained with 20 at. % Mg incorporation in the ZnO (Figure S2b, Supporting Information) because higher Mg contents leads to reduced current-densities, which offset the increase in the V_{OC}'s.

Second, we examined how charge can be transported through a Schottky barrier without rectification like an ohmic contact. Using impedance spectroscopy, the $Zn_{1-x}Mg_xO$/ITO interface was found to form a Schottky barrier, as is evident from the large parallel resistance in its Nyquist plot in Figure 2a. It

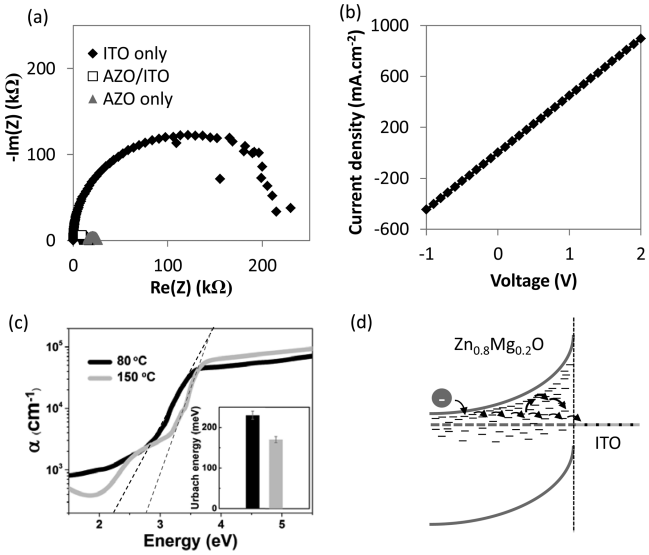

Figure 2. Electron transport through the $Zn_{0.8}Mg_{0.2}O$/TCO contact. (a) Nyquist plot comparing $Zn_{0.8}Mg_{0.2}O$/(60 nm) ITO with $Zn_{0.8}Mg_{0.2}O$/(30 nm) AZO/(60 nm) ITO with $Zn_{0.8}Mg_{0.2}O$/(70 nm) AZO. Ca/Ag was used to form an ohmic contact with $Zn_{1-x}Mg_xO$ in these measurements. (b) J−V plot of $Zn_{0.8}Mg_{0.2}O$/ITO. (c) Absorption spectra for $Zn_{0.8}Mg_{0.2}O$ deposited at 80 °C obtained using photothermal deflection spectroscopy (PDS). For comparison, the PDS absorption spectrum of $Zn_{0.8}Mg_{0.2}O$ deposited at 150 °C is also shown along with the respective Urbach energies obtained by fitting the band-tail. (d) Band diagram illustrating the hopping mechanism for electron transport through the Schottky barrier via states in the conduction band-tail of $Zn_{0.8}Mg_{0.2}O$ deposited at 80 °C to the conduction band of ITO.

should follow that if electrons need to overcome a Schottky barrier in order to be injected from the $Zn_{0.8}Mg_{0.2}O$ to the ITO, the current density−voltage (J−V) curve should display rectifying behavior.[25] Unexpectedly, this rectification is absent, with a linear J−V plot (Figure 2b) exhibited.[26] A linear J−V curve in the presence of a Schottky barrier may be due to (i) the $Zn_{0.8}Mg_{0.2}O$ Fermi level being pinned by surface states, leading to no band-bending,[26,27] (ii) the potential difference between $Zn_{0.8}Mg_{0.2}O$ and ITO being screened as a result of surface dipoles introduced by localized surface states[27] or (iii) charge tunneling through the Schottky barrier, either directly or via trap states extending below the band-edge of the $Zn_{0.8}Mg_{0.2}O$.[8,27] Fermi level pinning is unlikely,because there is a large parallel resistance at the $Zn_{0.8}Mg_{0.2}O$/ITO junction observed from impedance spectroscopy. Likewise, it is unlikely that surface dipoles are reducing the effective Schottky barrier since the Schottky barrier height between $Zn_{0.8}Mg_{0.2}O$ and ITO was measured to be 0.9 eV (Figure S3, Supporting Information) and this correlates well with the expected energy

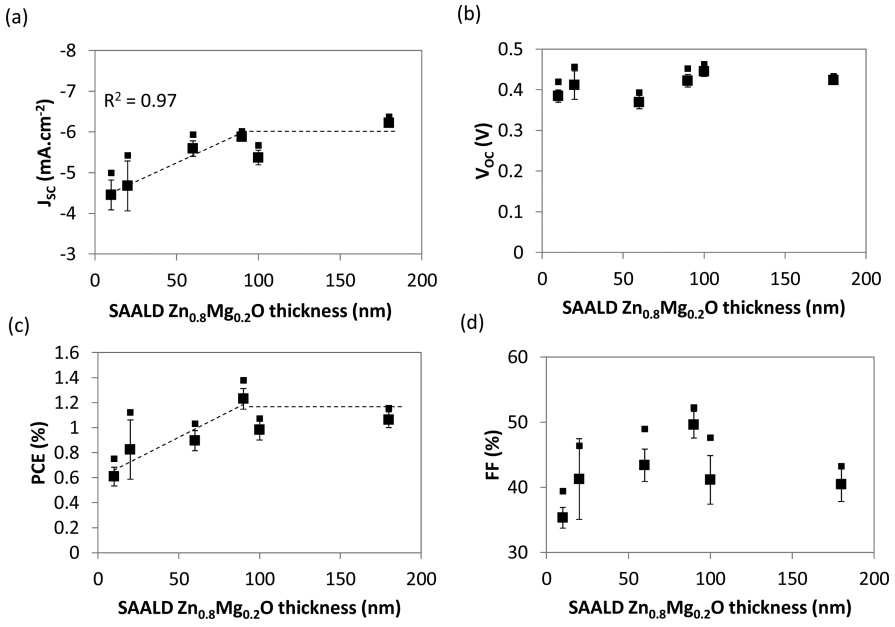

Figure 3. Variation in device performance with SAALD $Zn_{0.8}Mg_{0.2}O$ thickness. (a) Short-circuit current density (J_{SC}), (b) open-circuit voltage (V_{OC}), (c) efficiency (PCE) and (d) fill-factor (FF) vs SAALD $Zn_{0.8}Mg_{0.2}O$ thickness in devices with only ITO top contacts. Each data point is the average of at least five samples (highest measured values also shown). All devices were measured 1 day after fabrication.

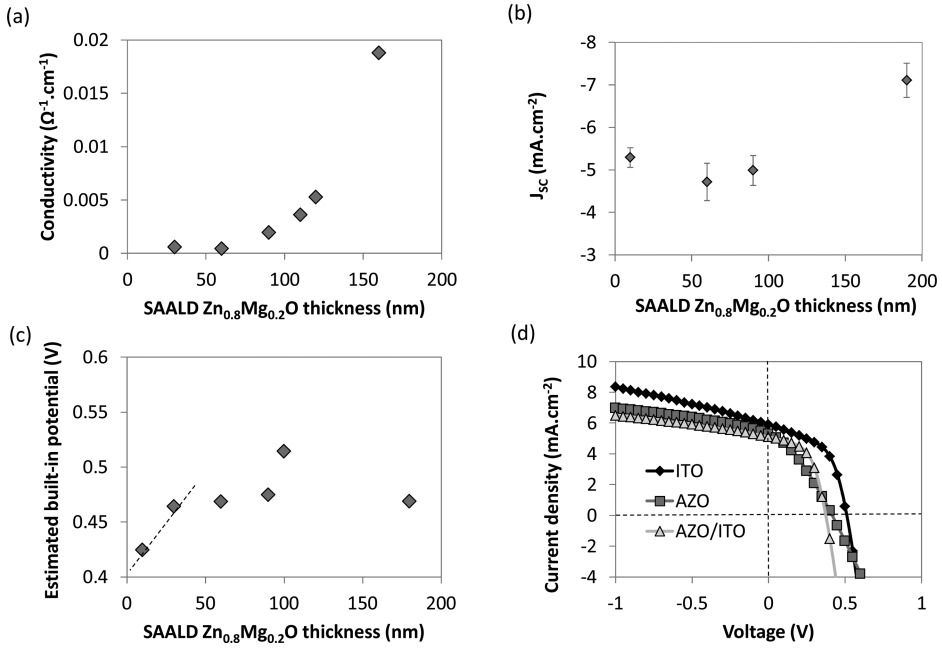

Figure 4. (a) Variation in the conductivity of SAALD $Zn_{0.8}Mg_{0.2}O$ films with thickness measured by four-point measurements. (b) Short-circuit current density (J_{SC}) vs SAALD $Zn_{0.8}Mg_{0.2}O$ thickness for devices with a 30 nm Al-doped ZnO (AZO) layer between the $Zn_{0.8}Mg_{0.2}O$ and ITO. Each data point is the average of 5−11 devices and measurements were performed on the same day as fabrication. (c) Built-in potential of the Cu_2O/$Zn_{0.8}Mg_{0.2}O$ *p*−*n* junction (for devices with ITO-only top contacts) estimated from light and dark *J*−*V* curves. (d) Light *J*−*V* curves of glass/ITO/(2.5 μm) Cu_2O/(90 nm) SAALD $Zn_{0.8}Mg_{0.2}O$/TCO devices measured under AM 1.5G illumination corrected for spectral mismatch. The TCOs compared are 60 nm ITO, 70 nm AZO, and 30 nm AZO with 60 nm ITO. Devices were measured immediately after fabrication.

level offset between $Zn_{0.8}Mg_{0.2}O$ (conduction band minimum at ∼−3.5 eV)[8] and ITO (workfunction of ∼−4.4 eV).[28] The Schottky barrier width between $Zn_{0.8}Mg_{0.2}O$ and ITO was calculated to range over 20−50 nm (or an average of 30 nm, and is calculated in Section S3 of the Supporting Information) and current cannot tunnel through a Schottky barrier of such height and width to a magnitude that is consistent with the photocurrent observed in these devices (Supporting Information, Section S2 and Figure S4). However, transport via a tunneling process may be possible if there exists a sufficiently high density of sub-bandgap states in the Schottky barrier depletion width that electrons can tunnel (hop) between. Accordingly, absorption measurements of $Zn_{0.8}Mg_{0.2}O$ (deposited at 80 °C) show the presence of a high density of sub-bandgap states in the metal oxide film (Figure 2c), which would be due to a high level of disorder, as can be seen from the high

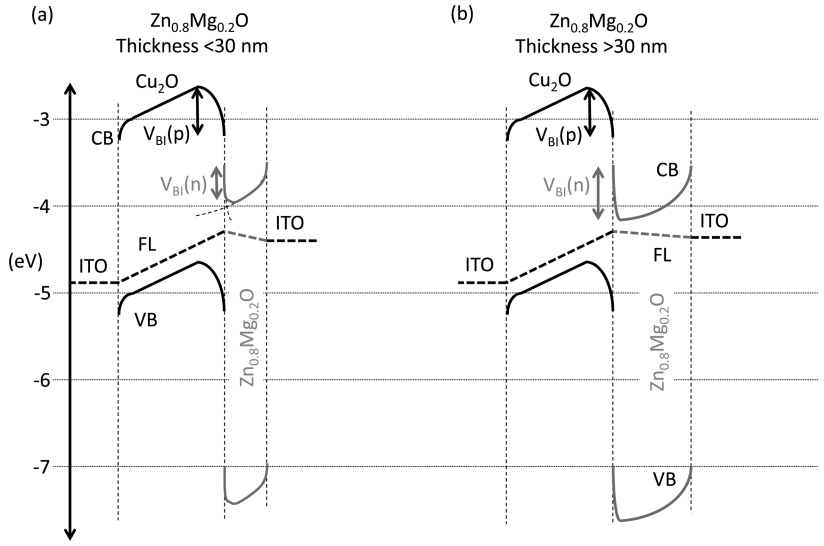

Figure 5. Band-diagram of ITO/Cu_2O/SAALD $Zn_{0.8}Mg_{0.2}O$/ITO with thin (<30 nm) and thick (>30 nm) $Zn_{0.8}Mg_{0.2}O$. (a) The $Zn_{0.8}Mg_{0.2}O$ is thinner than the full depletion width of the $Zn_{0.8}Mg_{0.2}O$/ITO Schottky barrier, and so the full built-in potential at the *p*−*n* junction cannot form. By (b) making the $Zn_{0.8}Mg_{0.2}O$ at least as thick as the Schottky barrier full depletion width (i.e., >30 nm), the full built-in potential of the *p*−*n* junction can form, leading to increased current densities. CB is the conduction band, VB the valence band and FL the Fermi level.

Urbach energy of 230 meV (compared with 170 meV for $Zn_{0.8}Mg_{0.2}O$ deposited at 150 °C).[8,29] This high level of disorder is partly due to the lack of preferred orientation in the $Zn_{0.8}Mg_{0.2}O$ films deposited at 80 °C (Figure 1d). By contrast, the 150 °C deposited $Zn_{0.8}Mg_{0.2}O$ is predominantly *a*-axis oriented (Figure 1d), which, in addition to its higher crystallinity, leads to a lower level of disorder.

To obtain current densities similar to those measured in $Cu_2O/Zn_{0.8}Mg_{0.2}O$/ITO devices reported here through tunneling, the tunneling barrier must be approximately 5 nm (Figure 3a and Figure S4 in the Supporting Information). The density of trap states was approximated from the inverse of the sub-bandgap absorption coefficients (Supporting Information, Section S2). The spacing between absorption centers in the band-edge was estimated to be ∼0.3 nm based on the spacing between the Γ-points of the Brillouin zones, because ZnO is a direct bandgap semiconductor with the bandgap transition at this point.[30] The absorption coefficient decreases by approximately 1 order of magnitude at 1 eV below the band-edge for $Zn_{0.8}Mg_{0.2}O$ deposited at 80 °C (Figure 2c), and this correlates with a trap spacing of ∼4 nm (Figure S6, Supporting Information). The spacing of sub-bandgap states extending up to 1 eV beneath the band-edge is therefore small enough for electrons to tunnel (hop) between adjacent states. Sub-bandgap states thus offer an alternative pathway for electrons to be transported through the $Zn_{0.8}Mg_{0.2}O$/ITO Schottky barrier and be directly injected into the ITO conduction band, as illustrated in Figure 2d.

This trap-facilitated method of charge transport through a Schottky barrier is similar to that found for ZnO/Au, in which the *I*−*V* curves changed from showing a Schottky junction to showing a junction behaving like an ohmic contact when defect states were present in the ZnO.[31] We also note that Cu_2O electrodeposited on ITO forms a Schottky interface, but behaves like an ohmic contact because Cu_2O has a high density of sub-bandgap states, allowing a similar hopping mechanism as discussed above for $Zn_{0.8}Mg_{0.2}O$ (Figure S7, Supporting Information). Whereas in our previous work we showed that metal oxide band-tails at heterojunctions limit open-circuit voltages,[8] this work shows that those band-tails are needed at Schottky interfaces to allow charge transport without rectification. Engineering the band-tail length to achieve a balance between the two effects is an important consideration for the future design of metal oxide solar cells.

Finally, to better understand the influence of the $Zn_{0.8}Mg_{0.2}O$/ITO Schottky barrier on device performance, we varied the $Zn_{0.8}Mg_{0.2}O$ thickness and found that the J_{SC}'s and efficiencies were strongly thickness-dependent for films thinner than 90 nm (Figures 3a,c). This effect may be due to (i) the electrical conductivity of $Zn_{0.8}Mg_{0.2}O$ increasing with thickness or (ii) the Schottky barrier reducing charge flow or (iii) the optical spacer effect.[32] These are separately examined in turn.

Using four-point measurements, we found that the conductivity of the SAALD $Zn_{0.8}Mg_{0.2}O$ films increased with thickness for films >60 nm (Figure 4a). This would lead to increased J_{SC}'s due to a decreasing series resistance. Photoluminescence measurements suggest that the increase in conductivity with film thickness is not fully accounted for by a carrier concentration change and we therefore deduce it to be mainly due to an increase in electron mobility, especially for films thicker than 60 nm (Figures S8 and S9, Supporting Information). However, it can be seen through a comparison of Figures 4a and 3a that a changing $Zn_{0.8}Mg_{0.2}O$ conductivity does not account for all of the observed J_{SC} change with thickness because the conductivities do not change for films thinner than 60 nm, whereas the J_{SC}'s change significantly.

To examine whether the $Zn_{0.8}Mg_{0.2}O$/ITO Schottky barrier influences the J_{SC}'s in the <90 nm thickness range, similar devices were made with 30 nm AZO inserted between the $Zn_{0.8}Mg_{0.2}O$ and ITO. It can be seen from the Nyquist plot in Figure 2a that this AZO layer forms an ohmic contact with $Zn_{0.8}Mg_{0.2}O$. Figure 4b shows that with an ohmic contact, the trend in J_{SC} with increasing SAALD $Zn_{0.8}Mg_{0.2}O$ thickness follows the trend in film conductivity but, importantly, the J_{SC}'s do not drop off for films thinner than 30 nm. This strongly suggests that the decrease in J_{SC} for films thinner than 30 nm is a result of the Schottky barrier.

For such a claim that the Schottky barrier is influencing the current densities to hold true, the Schottky barrier width must be at or near the 30 nm cutoff point. The barrier width can be estimated from the Poisson equation, where full carrier depletion is assumed,[33] and is estimated to be between 20 and 50 nm (see the Supporting Information, Section S3). Thus, when the films are 30 nm or thinner, the band-bending due to the Schottky barrier should overlap with the band-bending at the $p-n$ junction and therefore reduce the built-in potential (Figure 5a). To verify this concept, the built-in potentials (V_{BI}) were estimated from the voltage at which the light and dark current densities are equal (Figure 4c). It can be seen that there was an increase in the V_{BI} from the 10 to 30 nm thick films. The series resistance of the devices was 20−40 Ω·cm^2, from which a 0.04 V increase in the V_{BI} corresponds to a maximum increase of 1.3 mA·cm^{-2} in the J_{SC} (calculation given in Section S3 of the Supporting Information), which more than accounts for the increase in J_{SC} that occurred (Figure 3a). Thus, spacing the Schottky barrier away from the $p-n$ junction allows a larger built-in potential to form at the heterojunction (Figure 5b), producing a larger driving force for electrons to overcome the series resistance of the device. The V_{BI} change is not large enough compared to the factors governing the V_{OC} loss mechanisms to lead to a significant change in the V_{OC} in Figure 3b.

Finally, to evaluate whether the optical spacer effect accounts for the J_{SC} changing with thickness, a transfer matrix model[34] was employed to calculate the maximum J_{SC} from the solar cells. It was found that the modeled change in the J_{SC} with thickness is less than 0.5 mA·cm^{-2} (Figure S10a, Supporting Information), which does not account for the >1 mA·cm^{-2} change in J_{SC} observed.

The change in fill factors (FFs) in Figure 3d relates to the influence of the Schottky barrier, $Zn_{0.8}Mg_{0.2}O$ conductivity and device fabrication on recombination. When the Schottky barrier is closer to the heterojunction than its depletion width (<30 nm thick $Zn_{0.8}Mg_{0.2}O$), it opposes electron-injection, which therefore increases interfacial recombination and decreases FFs.[1] On the other hand, the increasing film conductivity for devices with $Zn_{0.8}Mg_{0.2}O$ thicker than 30 nm (with reducing series resistance) allows a greater fraction of injected charges to be extracted before they recombine in the bulk of the $Zn_{0.8}Mg_{0.2}O$ window layer.[8] For thicknesses of $Zn_{0.8}Mg_{0.2}O$ larger than 90 nm, a decrease in FF is observed in Figure 3d. The reason for this is likely related to the prolonged heating of the Cu_2O at 80 °C due to the longer deposition time required to produce thicker metal oxide films. This could have two effects: (i) creation of a thicker surface layer of CuO, which can enhance interfacial recombination[19,20] or (ii) the creation of microcracks in Cu_2O arising from the different thermal expansion of the Cu_2O across its thickness. If these microcracks are introduced, they can act as shunt pathways that increase recombination and reduce FFs.[15,35]

Overall, ITO-only top contacts led to better performance than devices with AZO. By mitigating the effects of the $Zn_{0.8}Mg_{0.2}O$/ITO Schottky barrier, an efficiency of 1.6% (Figure 4d) was achieved. This is double that obtained using a 70 nm AZO TCO, and is also 50% higher than the efficiency of 1.07% obtained using a (30 nm) AZO/(60 nm) ITO top transparent contact. The main reason for these improved performances is a higher J_{SC}, arising from the low resistivity of ITO ($(7 \pm 1) \times 10^{-4}$ Ω·cm) compared with AZO (0.8 Ω·cm), which is consistent with reports in the literature.[36] The J_{SC} of −6.2 mA·cm^{-2} obtained using ITO as the top contact is higher than J_{SC}'s typically obtained using a bilayer device with electrochemically deposited Cu_2O with the $p-n$ junction fabricated in open-air (3.8−4.5 mA·cm^{-2}).[9,15,22,24] We also note that 1.6% is the highest efficiency obtained from an electrochemically deposited Cu_2O device with a $p-n$ junction fabricated using open-air techniques.[24]

CONCLUSION

In summary, we have shown that it is possible to overcome the performance-reducing effects of Schottky barriers between $Zn_{1-x}Mg_xO$ and ITO, allowing higher current densities to be obtained and efficiencies that were double those obtained using ohmic AZO contacts. Charge transport through the $Zn_{1-x}Mg_xO$/ITO Schottky barrier without rectification (like an ohmic contact) was found to occur via charge hopping through states in the $Zn_{1-x}Mg_xO$ band-tail. The extent to which the $Zn_{1-x}Mg_xO$/ITO Schottky barrier limits current densities is minimized by spacing it away from the $p-n$ junction to allow the full built-in potential to form while simultaneously increasing the conductivity of the films. By showing that transparent conducting electrodes do not need to have matching Fermi levels with the metal oxides they are in contact with, this work has important implications for the design of new generation solar cells, thus providing greater flexibility in the selection of electrode materials.

ASSOCIATED CONTENT

Supporting Information

Photovoltaic measurements for the optimization of SAALD $Zn_{1-x}Mg_xO$ composition and deposition conditions onto Cu_2O, analysis of $Zn_{1-x}Mg_xO$/ITO and Cu_2O/ITO interfaces to determine how charge can be transported through a Schottky barrier without rectification, supporting measurements for the analysis of the reasons for the change in current density of $Cu_2O-Zn_{0.8}Mg_{0.2}O$ devices with $Zn_{0.8}Mg_{0.2}O$ thickness. This material is available free of charge via the Internet at http://pubs.acs.org.

AUTHOR INFORMATION

Corresponding Author

*K. P. Musselman. E-mail: kpdm2@cam.ac.uk.

Notes

The authors declare no competing financial interest.

ACKNOWLEDGMENTS

The authors acknowledge useful discussions with Dr. Talia S. Gershon and the assistance of Dr. Nadia Stelmashenko. This work was supported by the Cambridge Commonwealth, European and International Trusts and Rutherford Foundation of New Zealand, EPSRC of the UK (award number RG3717) and the University of Cambridge EPSRC Centre for Doctoral Training in Nanoscience, ERC Advanced Investigator Grant, Novox, ERC-2009-adG247276 and Girton College Cambridge.

REFERENCES

(1) Demtsu, S. H.; Sites, J. R. Effect of Back-Contact Barrier on Thin-Film CdTe Solar Cells. *Thin Solid Films* **2006**, *510*, 320−324.

(2) Chuang, C.-H. M.; Brown, P. R.; Bulović, V.; Bawendi, M. G. Improved Performance and Stability in Quantum Dot Solar Cells through Band Alignment Engineering. *Nat. Mater.* **2014**, *13*, 796−801.

(3) Marin, A. T.; Musselman, K. P.; MacManus-Driscoll, J. L. Accurate Determination of Interface Trap State Parameters by

Admittance Spectroscopy in the Presence of a Schottky Barrier Contact: Application to ZnO-based Solar Cells. *J. Appl. Phys.* **2013**, *113*, 144502.
(4) Olson, D. C.; Shaheen, S. E.; White, M. S.; Mitchell, W. J.; van Hest, M. F. A. M.; Collins, R. T.; Ginley, D. S. Band-Offset Engineering for Enhanced Open-Circuit Voltage in Polymer−Oxide Hybrid Solar Cells. *Adv. Funct. Mater.* **2007**, *17*, 264−269.
(5) Hoye, R. L. Z.; Musselman, K. P.; MacManus-Driscoll, J. L. Doping ZnO and TiO_2 for Solar Cells. *APL Mater.* **2013**, *1*, 060701.
(6) Kumar, A.; Zhou, C. The Race to Replace Tin-Doped Indium Oxide: Which Material Will Win? *ACS Nano* **2010**, *4*, 11−14.
(7) Hoye, R. L. Z.; Muñoz-Rojas, D.; Iza, D. C.; Musselman, K. P.; MacManus-Driscoll, J. L. High Performance Inverted Bulk Heterojunction Solar Cells by Incorporation of Dense, Thin ZnO Layer Made Using Atmospheric Atomic Layer Deposition. *Sol. Energy Mater. Sol. Cells* **2013**, *116*, 197−202.
(8) Hoye, R. L. Z.; Ehrler, B.; Böhm, M. L.; Muñoz-Rojas, D.; Altamimi, R. M.; Alyamani, A. Y.; Vaynzof, Y.; Sadhanala, A.; Ercolano, G.; Greenham, N. C.; Friend, R. H.; MacManus-Driscoll, J. L.; Musselman, K. P. Improved Open-Circuit Voltage in ZnO-PbSe Quantum Dot Solar Cells by Understanding and Reducing Losses Arising from the ZnO Conduction Band Tail. *Adv. Energy Mater.* **2014**, *4*, 1301544.
(9) Musselman, K. P.; Wisnet, A.; Iza, D. C.; Hesse, H. C.; Scheu, C.; MacManus-Driscoll, J. L.; Schmidt-Mende, L. Strong Efficiency Improvements in Ultra-Low-Cost Inorganic Nanowire Solar Cells. *Adv. Mater.* **2010**, *22*, E254−E258.
(10) Sarkar, K.; Braden, E. V.; Pogorzalek, S.; Yu, S.; Roth, S. V.; Müller-Buschbaum, P. Monitoring Structural Dynamics of in Situ Spray-Deposited Zinc Oxide Films for Application in Dye-Sensitized Solar Cells. *ChemSusChem* **2014**, *7*, 2140−2145.
(11) Musselman, K. P.; Albert-Seifried, S.; Hoye, R. L. Z.; Sadhanala, A.; Muñoz-Rojas, D.; MacManus-Driscoll, J. L.; Friend, R. H. Improved Exciton Dissociation at Semiconducting Polymer:ZnO Donor:Acceptor Interfaces via Nitrogen Doping of ZnO. *Adv. Funct. Mater.* **2014**, *24*, 3562−3570.
(12) Yaklin, M. A.; Schneider, D. A.; Norman, K.; Granata, J. E.; Staiger, C. L. Impacts of Humidity and Temperature on the Performance of Transparent Conducting Zinc Oxide. In *Proceedings of the 35th Photovoltaic Specialists Conference (PVSC)*, Honolulu, HI, June 20−25, 2010; IEEE: New York, 2010; pp 002493−002496.
(13) Cao, Q.; Gunawan, O.; Copel, M.; Reuter, K. B.; Chey, S. J.; Deline, V. R.; Mitzi, D. B. Defects in $Cu(In,Ga)Se_2$ Chalcopyrite Semiconductors: A Comparative Study of Material Properties, Defect States, and Photovoltaic Performance. *Adv. Energy Mater.* **2011**, *1*, 845−853.
(14) Todorov, T. K.; Reuter, K. B.; Mitzi, D. B. High-Efficiency Solar Cell with Earth-Abundant Liquid-Processed Absorber. *Adv. Mater.* **2010**, *22*, E156−E159.
(15) Gershon, T.; Musselman, K. P.; Marin, A.; Friend, R. H.; MacManus-Driscoll, J. L. Thin-Film ZnO/Cu_2O Solar Cells Incorporating an Organic Buffer Layer. *Sol. Energy Mater. Sol. Cells* **2012**, *96*, 148−154.
(16) Lee, Y. S.; Heo, J.; Siah, S. C.; Mailoa, J. P.; Brandt, R. E.; Kim, S. B.; Gordon, R. G.; Buonassisi, T. Ultrathin Amorphous Zinc-Tin-Oxide Buffer Layer for Enhancing Heterojunction Interface Quality in Metal-Oxide Solar Cells. *Energy Environ. Sci.* **2013**, *6*, 2112−2114.
(17) Sarkar, K.; Braden, E. V.; Fröschl, T.; Hüsing, N.; Müller-Buschbaum, P. Spray-Deposited Zinc Titanate Films Obtained via Sol−Gel Synthesis for Application in Dye-Sensitized Solar Cells. *J. Mater. Chem. A* **2014**, *2*, 15008−15014.
(18) Musselman, K. P.; Marin, A.; Schmidt-Mende, L.; MacManus-Driscoll, J. L. Incompatible Length Scales in Nanostructured Cu_2O Solar Cells. *Adv. Funct. Mater.* **2012**, *22*, 2202−2208.
(19) Ievskaya, Y.; Hoye, R. L. Z.; Sadhanala, A.; Musselman, K. P.; MacManus-Driscoll, J. L. Fabrication of ZnO/Cu_2O Heterojunctions in Atmospheric Conditions: Improved Interface Quality and Solar Cell Performance. *Sol. Energy Mater. Sol. Cells* **2014**, DOI: 10.1016/j.solmat.2014.09.018.
(20) Lee, S. W.; Lee, Y. S.; Heo, J.; Siah, S. C.; Chua, D.; Brandt, R. E.; Kim, S. B.; Mailoa, J. P.; Buonassisi, T.; Gordon, R. G. Improved Cu_2O-based Solar Cells Using Atomic Layer Deposition to Control the Cu Oxidation State at the p-n Junction. *Adv. Energy Mater.* **2014**, *4*, 1301916.
(21) Lee, Y. S.; Chua, D.; Brandt, R. E.; Siah, S. C.; Li, J. V.; Mailoa, J. P.; Lee, S. W.; Gordon, R. G.; Buonassisi, T. Atomic Layer Deposited Gallium Oxide Buffer Layer Enables 1.2 V Open-Circuit Voltage in Cuprous Oxide Solar Cells. *Adv. Mater.* **2014**, *26*, 4704−4710.
(22) Izaki, M.; Shinagawa, T.; Mizuno, K.-T.; Ida, Y.; Inaba, M.; Tasaka, A. Electrochemically Constructed P-Cu_2O/N-ZnO Heterojunction Diode for Photovoltaic Device. *J. Phys. D.: Appl. Phys.* **2007**, *40*, 3326−3329.
(23) Duan, Z.; Du Pasquier, A.; Lu, Y.; Xu, Y.; Garfunkel, E. Effects of Mg Composition on Open Circuit Voltage of Cu_2O−$Mg_xZn_{1-x}O$ Heterojunction Solar Cells. *Sol. Energy Mater. Sol. Cells* **2012**, *96*, 292−297.
(24) Fujimoto, K.; Oku, T.; Akiyama, T. Fabrication and Characterization of ZnO/Cu_2O Solar Cells Prepared by Electrodeposition. *Appl. Phys. Express* **2013**, *6*, 086503.
(25) Yoon, J.-G.; Cho, S. W.; Lee, E.; Chung, J.-S. Characteristics of Indium-Tin-Oxide Schottky Contacts to ZnMgO/ZnO Heterojunctions with Band Gap Grading. *Appl. Phys. Lett.* **2009**, *95*, 222102.
(26) Brown, P. R.; Lunt, R. R.; Zhao, N.; Osedach, T. P.; Wanger, D. D.; Chang, L.-Y.; Bawendi, M. G.; Bulović, V. Improved Current Extraction from ZnO/PbS Quantum Dot Heterojunction Photovoltaics Using a MoO_3 Interfacial Layer. *Nano Lett.* **2011**, *11*, 2955−2961.
(27) Brillson, L. J.; Lu, Y. ZnO Schottky Barriers and Ohmic Contacts. *J. Appl. Phys.* **2011**, *109*, 121301.
(28) Park, Y.; Choong, V.; Gao, Y.; Hsieh, B. R.; Tang, C. W. Work Function of Indium Tin Oxide Transparent Conductor Measured by Photoelectron Spectroscopy. *Appl. Phys. Lett.* **1996**, *68*, 2699.
(29) Sadhanala, A.; Deschler, F.; Thomas, T. H.; Dutton, E.; Goedel, K. C.; Hanusch, F. C.; Lai, M. L.; Steiner, U.; Bein, T.; Docampo, P.; Cahen, D.; Friend, R. H. Preparation of Single-Phase Films of $CH_3NH_3Pb(I_{1-x}Br_x)_3$ with Sharp Optical Edges. *J. Phys. Chem. Lett.* **2014**, *5*, 2501−2505.
(30) Bundesmann, C.; Schmidt-Grund, R.; Schubert, M. In *Transparent Conductive Zinc Oxide: Basics and Applications in Solar Cells*; Ellmer, K., Klein, A., Bernd, R., Eds.; Springer: Heidelberg, Germany, 2008; Chapter 3, pp 79−124.
(31) Brillson, L. J.; Mosbacker, H. L.; Hetzer, M. J.; Strzhemechny, Y.; Jessen, G. H.; Look, D. C.; Cantwell, G.; Zhang, J.; Song, J. J. Dominant Effect of Near-Interface Native Point Defects on ZnO Schottky Barriers. *Appl. Phys. Lett.* **2007**, *90*, 102116.
(32) Kim, J. Y.; Kim, S. H.; Lee, H.-H.; Lee, K.; Ma, W.; Gong, X.; Heeger, A. J. New Architecture for High-Efficiency Polymer Photovoltaic Cells Using Solution-based Titanium Oxide as an Optical Spacer. *Adv. Mater.* **2006**, *18*, 572−576.
(33) Stallinga, P. *Electrical Characterization of Organic Electronic Materials and Devices*, 1st ed; John Wiley & Sons Ltd: West Sussex, U. K., 2009.
(34) Burkhard, G. F.; Hoke, E. T.; McGehee, M. D. Accounting for Interference, Scattering, and Electrode Absorption to Make Accurate Internal Quantum Efficiency Measurements in Organic and Other Thin Solar Cells. *Adv. Mater.* **2010**, *22*, 3293−3297.
(35) Zhang, K.; Rossi, C.; Tenailleau, C.; Alphonse, P.; Chane-Ching, J.-Y. Synthesis of Large-Area and Aligned Copper Oxide Nanowires from Copper Thin Film on Silicon Substrate. *Nanotechnology* **2007**, *18*, 275607.
(36) Mereu, R. A.; Marchionna, S.; Le Donne, A.; Ciontea, L.; Binetti, S.; Acciarri, M. Optical and Electrical Studies of Transparent Conductive AZO and ITO Sputtered Thin Films for CIGS Photovoltaics. *Phys. Status Solidi C* **2014**, *11*, 1464−1467.